Intracellular Ca²⁺ Oscillations, a Potential Pacemaking Mechanism in Early Embryonic Heart Cells

Philipp Sasse,[1] Jianbao Zhang,[2,3] Lars Cleemann,[4] Martin Morad,[4] Juergen Hescheler,[2] and Bernd K. Fleischmann[1]

[1]Institute of Physiology I, Life and Brain Center, University of Bonn, Bonn 53105, Germany
[2]Institute of Neurophysiology, University of Cologne, Cologne 50931, Germany
[3]Institute of Biomedical Engineering, Xi´an Jiaotong University, Xi´an 710049, China
[4]Department of Pharmacology, Georgetown University Medical Center, Washington, DC 20057

Early (E9.5–E11.5) embryonic heart cells beat spontaneously, even though the adult pacemaking mechanisms are not yet fully established. Here we show that in isolated murine early embryonic cardiomyocytes periodic oscillations of cytosolic Ca^{2+} occur and that these induce contractions. The Ca^{2+} oscillations originate from the sarcoplasmic reticulum and are dependent on the IP_3 and the ryanodine receptor. The Ca^{2+} oscillations activate the Na^+-Ca^{2+} exchanger, giving rise to subthreshold depolarizations of the membrane potential and/or action potentials. Although early embryonic heart cells are voltage-independent Ca^{2+} oscillators, the generation of action potentials provides synchronization of the electrical and mechanical signals. Thus, Ca^{2+} oscillations pace early embryonic heart cells and the ensuing activation of the Na^+-Ca^{2+} exchanger evokes small membrane depolarizations or action potentials.

INTRODUCTION

Generation of spontaneous electrical activity in the adult sinoatrial node depends on a delicate interplay between different ionic conductances, exchanger activities, and ATPases. Voltage-dependent Ca^{2+} channels (Shih, 1994; Schram et al., 2002) and hyperpolarization-activated nonselective cation channels (HCN) (Baruscotti and DiFrancesco, 2004; Stieber et al., 2003) are thought to underlie the diastolic depolarization. In addition, recent data suggest that also Ca^{2+} release from the SR plays a role in modulating the rate of the diastolic depolarization by activating the Na^+-Ca^{2+} exchanger (NCX) (Vinogradova et al., 2004; Maltsev et al., 2006). The spontaneous electrical activity is propagated throughout the heart via specialized cells of the conduction system. Adult cardiomyocytes are coupled to the conduction system through gap junctions and the contraction is regulated by the L-type Ca^{2+} current–gated Ca^{2+} release from the SR, a mechanism called Ca^{2+}-induced Ca^{2+} release (CICR) (Fabiato, 1983; Adachi-Akahane et al., 1996).

While in the adult heart, pacemaker, atrial, and ventricular cardiomyocytes are specialized cells with different morphology and specific physiological functions, these differences are less pronounced in the early developing heart (Maltsev et al., 1994). Using embryonic stem (ES) cell–derived and embryonic cardiomyocytes we and others have shown that these cells are spontaneously active

although the ionic conductances responsible for pacemaking in the adult heart are either not or only partially expressed (Kolossov et al., 1998; Abi-Gerges et al., 2000; Bony et al., 2001; Fleischmann et al., 2004; Kolossov et al., 2005). Furthermore, transgenic mice deficient in principal components of the pacemaking machinery such as $Ca_v1.2$ (Seisenberger et al., 2000) and HCN4 (Stieber et al., 2003) were found to display spontaneous beating at early embryonic stages (E8.5–E10.5), indicating that alternative mechanisms for automaticity exist in the embryonic heart.

Our and others previous work in ES cell–derived pacemaker-like cells showed that spontaneous beating persisted in high extracellular K^+ solution, suggesting that this might be related to oscillations of the cytosolic Ca^{2+} concentration ($[Ca^{2+}]_i$) (Viatchenko-Karpinski et al., 1999) and that these oscillations are inositol-1,4,5-trisphosphate (IP_3) dependent (Mery et al., 2005). However, these earlier studies are inconclusive regarding the mechanism(s) responsible for the generation of beating since at the early embryonic stage, besides pacemaker cells, atrial and ventricular cells are also spontaneously active.

Therefore, the aim of our study was to unravel the cellular mechanisms responsible for the initiation of

---

Correspondence to Bernd K. Fleischmann:
bernd.fleischmann@uni-bonn.de

The online version of this article contains supplemental material.

Abbreviations used in this paper: AP, action potential; CICR, Ca^{2+}-induced Ca^{2+} release; ES, embryonic stem; FFT, fast Fourier transformation; IP_3, inositol-1,4,5-trisphosphate; IP_3R, IP_3 receptor; MDP, maximum diastolic potential; NCX, Na^+-Ca^{2+} exchanger; TTX, tetrodotoxin; 2-APB, 2-aminoethyl diphenyl borate.
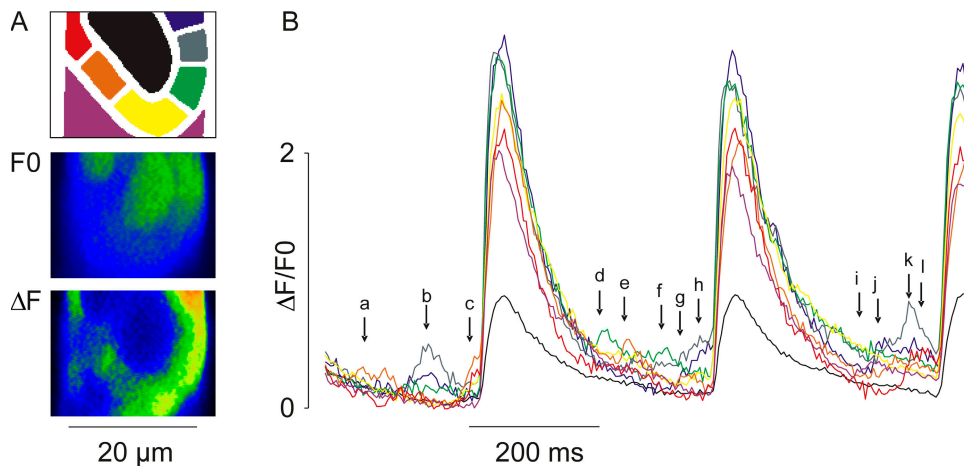
Figure 1. Fast 2D confocal imaging identifies small localized $[Ca^{2+}]_i$ release events. (A) Mid section of an E10 embryonic cell imaged using 2D confocal fluorescence microscopy at 240 frames/s. (Top) Diagram showing regions subjected to measurements of average fluorescence intensity (black = nuclear region; blue, olive, green, yellow, orange, red = perinuclear regions; purple = remaining cytoplasmic region). F0 shows average fluorescence intensity during the diastolic intervals while ΔF represents the synchronous increase in $[Ca^{2+}]_i$-dependent fluorescence associated with spontaneous repetitive APs. (B) Regional changes in fluorescence intensity measured in 240 frames during a 1-s recording. Colors correspond to the subcellular regions indicated in A, top. Arrows indicate local $[Ca^{2+}]_i$ signals of low intensity occurring during diastolic intervals in different perinuclear regions as seen also in Fig. S1.

the spontaneous beating, the electrical excitability and synchronization of the excitation in the early embryonic heart. In distinction from the above mentioned earlier studies (Viatchenko-Karpinski S. et al., 1999; Mery et al., 2005) of ES cell–derived cells, we have used cardiomyocytes from early murine embryos. This model has distinct advantages as the different cardiac subtypes can be investigated and as all cells are at the same stage of differentiation. Moreover, we have combined $[Ca^{2+}]_i$ imaging and patch-clamp techniques to identify pacemaker mechanisms in early embryonic cardiac muscle cells.

MATERIALS AND METHODS

Cell Preparation
Mice of the strain HIM:OF1 or CD1 were superovulated and the hearts were harvested at the early embryonic stage (E8.5–E10.5) and isolated as reported earlier (Fleischmann et al., 2004; Herr et al., 2001). In brief, embryonic heart tubes were digested enzymatically using collagenase B (Roche Diagnostics) for 30 min. Single cells were cultivated for 48–72 h at 37°C on gelatine-covered glass coverslips in DMEM or Iscove-MEM supplemented with 10–20% FCS (Invitrogen), L-glutamine (2 mM), and nonessential amino acids (1%). The cells were cultured for 48–72 h after the dissociation in order to allow adhesion to the glass coverslips and recovery from enzymatic dissociation. Control experiments (Fig. S2, available at http://www.jgp.org/cgi/content/full/jgp.200609575/DC1) were performed with freshly dissociated embryonic cardiomyocytes within 6 h after isolation; fast adhesion to the glass coverslips was promoted by coating with laminin (1 μg/ml). We have not observed differences in the functional phenotype ($[Ca^{2+}]_i$ oscillations) of single cardiomyocytes harvested from murine hearts ranging from E8.5 to E10.5 and have therefore pooled the data.

Two-Dimensional Confocal $[Ca^{2+}]_i$ Imaging
Embryonic cells were loaded with the Ca^{2+} indicator dye fluo-3AM (2 μM, 15 min) and imaged using a Noran Odyssey XL 2-D laser scanning confocal microscopy system (Noran Instruments) as previously described (Cleemann et al., 1998; Woo et al., 2002). Images were scanned at 240 Hz, the data were acquired by the Intervision program in a workstation computer (IRIX-operating system, Indy, Silicon Graphics) and were analyzed with our own computer program (Con2i) written in Visual Basic 6.0 (Microsoft). Tracings of local $[Ca^{2+}]_i$ transients were measured from subcellular regions indicated as colored masks (see Fig. 1 A, top), and were shown as the increase in the average fluorescence of each frame normalized relative to the average resting fluorescence ($\Delta F/F_0$, Fig. 1 B).

Electrophysiology and $[Ca^{2+}]_i$ Imaging
Experiments were performed in a temperature-controlled recording chamber (35 ± 2°C) using an inverted microscope (Axiovert 135 or 200; Carl Zeiss MicroImaging, Inc.) with a 20× air or 40× oil immersion objective (Fluar; Carl Zeiss MicroImaging, Inc.). Only spontaneously beating cardiomyocytes were selected for the experiments. The electrophysiological recordings were performed as reported earlier (Fleischmann et al., 2004). In brief, the whole-cell patch-clamp configuration was employed in the voltage- or current-clamp mode. Data were digitized at 1–10 kHz and filtered at 1 kHz. Fast Fourier transformation (FFT) was performed using the FFT function of Origin 7.5 (OriginLab) with a Blackman window and the power displayed on a linear scale (Fig. 2, B and F). $[Ca^{2+}]_i$ imaging was performed as reported earlier (Herr et al., 2001). In brief, monochromic excitation light (340, 380 nm, 10 ms) was generated at a ratio frequency of 20–40 Hz by a computer-controlled monochromator. Emitted light was collected through a 470-nm long pass filter using a cooled digital CCD camera in 2*2 binning mode. In some experiments a LED was used to document beating simultaneously. Contraction was analyzed by peak detection of changes of gray levels in small contrast-rich areas of the cell.

We have used the classic whole-cell technique as very low access resistance and good control over the intracellular Na^+ concentration (10 mM) was important for stable recordings and to avoid blockage of the reverse mode of the NCX that occurs at low $[Na^+]_i$. A further advantage of this configuration was that the precise concentration of the exogenous buffer (Fura-2) was known. Experiments were started shortly (1–2 min) after rupturing the cell membrane because $[Ca^{2+}]_i$ oscillations proved sensitive to dialysis. We used 50 μM Fura-2 and 50 μM EGTA in the internal solution; without this slight buffering the cells tended to $[Ca^{2+}]_i$ overload and to irreversibly contract shortly after the whole cell configuration was achieved. The buffer capacitance of Fura-2 increased with experimental time and varied in different cells due
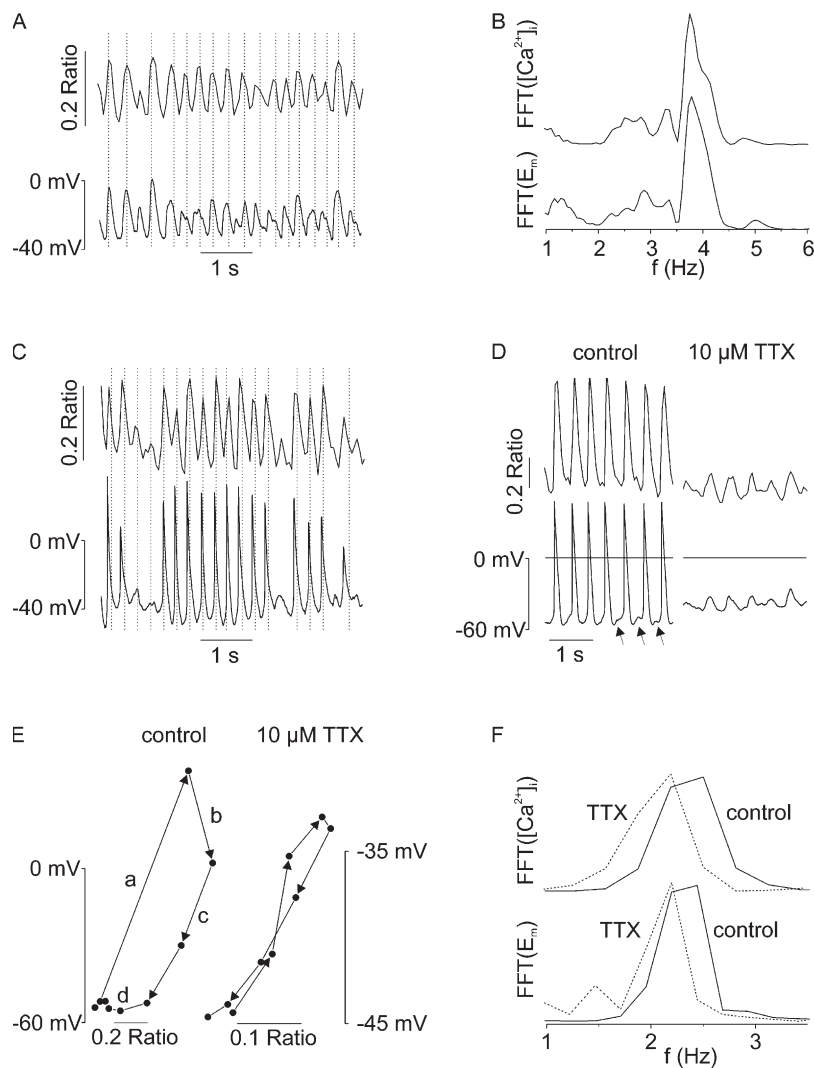
Figure 2. Early embryonic (E8.5–E10.5) cardio (A and C) Examples of cells with contractions (indicated by dashed lines) synchronous to $[Ca^{2+}]_i$ (top) and E_m (bottom) oscillations without (A) or with primitive APs (C). (B) Fast Fourier transformation (FFT) of $[Ca^{2+}]_i$ (top) and E_m (bottom) signals from Fig. 2 A revealed identical periodicity. (D) Application of the Na^+ channel inhibitor TTX in cells displaying APs and $[Ca^{2+}]_i$ transients (left) revealed the underlying basic rhythm of $[Ca^{2+}]_i$ and E_m oscillations (right). (E) Plotting the $[Ca^{2+}]_i$ signal of Fig. 2 D vs. E_m results in a hysteresis loop for a single AP (left) and a linear relation for a single $[Ca^{2+}]_i$ oscillation after application of TTX (right). For details on the four phases (a–d) see text. F: FFT of $[Ca^{2+}]_i$ (top) and E_m (bottom) signals from Fig. 2 D shows similar periodicity before (solid lines) and during application of TTX (dashed lines).

to different access through the patch pipette. Because of this and the somewhat uncertain K_d of Fura-2 in embryonic cardiomyocytes, we displayed the emission ratios upon 340 and 380 nm excitation with background subtraction of emitted light before the rupture of the cell membrane.

In some experiments where long and stable recording times were required (Fig. 4, B, C, and E; Fig. 5 F; and Fig. S2) cells were loaded with Fura-2-acetoxymethyl ester (Fura-2-AM, 2 µM, 12–15 min) and measured as described earlier (Herr et al., 2001). The ratios were calculated offline with subtraction of background intensities at both wavelengths for each frame individually. Since these cells showed the same behavior as the voltage-clamped cells, we include them in the statistics for Fig. 3 (B and C). Some of the cells (Fig. 4 E and Fig. 5 F) were investigated using the perforated patch-clamp technique (nystatin 150–500 µg/ml), since this allows long recording times without interference with $[Ca^{2+}]_i$ oscillations. To obtain more cells with action potentials (APs) in these experiments the low frequency voltage-clamp mode of the EPC10 amplifier was used to inject current to reach membrane potentials around −50 mV. For electrical field stimulation a custom built isolated stimulator (50 V, 2 ms) and two platinum electrodes were used. Acutely dissociated cells (Fig. S2) were Fura-2-AM loaded and investigated using the classic sharp micro-electrode technique with electrodes filled with 3 M KCl and with a resistance of 20–40 MΩ.

Solutions

Solutions were of the following composition (in mM): external, NaCl 140, KCl 5.4, CaCl$_2$ 1.8/2/3.6, MgCl$_2$ 1, glucose 10, HEPES 10, pH 7.4 (adjusted with NaOH). For some experiments Na^+ was replaced by isomolar concentrations of aspartate (Fig. 5, B and D) or Li^+ (Fig. 5 F; Fig. 6, C and F). Some recordings (Fig. 4, B, C, and E; Fig. 5, E and F; Fig. 7, E and F; Fig. S2) were performed in 1.8–2 mM external Ca^{2+}. The internal solution had the following composition: KCl 40, K-asparatate 90, NaCl 10, MgATP 3, MgCl$_2$ 1, HEPES 10, EGTA 0.05, K$_5$Fura-2 0.05, pH 7.2 (adjusted with KOH). For electrophysiological experiments without imaging (Fig. 6) K$_5$Fura-2 was omitted. Exchange of solutions was done with a custom-built rapid perfusion system allowing complete local solution exchange within 50 ms. Nifedipine and 2-aminoethyl diphenyl borate (2-APB; Sigma-Aldrich) were dissolved in ethanol and methanol (final concentration 0.1%); thapsigargin, ryanodine (Sigma-Aldrich), and Fura-2-AM (Molecular Probes) were dissolved in DMSO (final concentration <0.1%). Tetrodotoxin (TTX) was from Tocris, and all remaining substances were purchased from Sigma-Aldrich and dissolved to the final concentration in normal extracellular solution.

Online Supplemental Material

The online supplemental material (available at http://www.jgp .org/cgi/content/full/jgp.200609575/DC1) contains still images
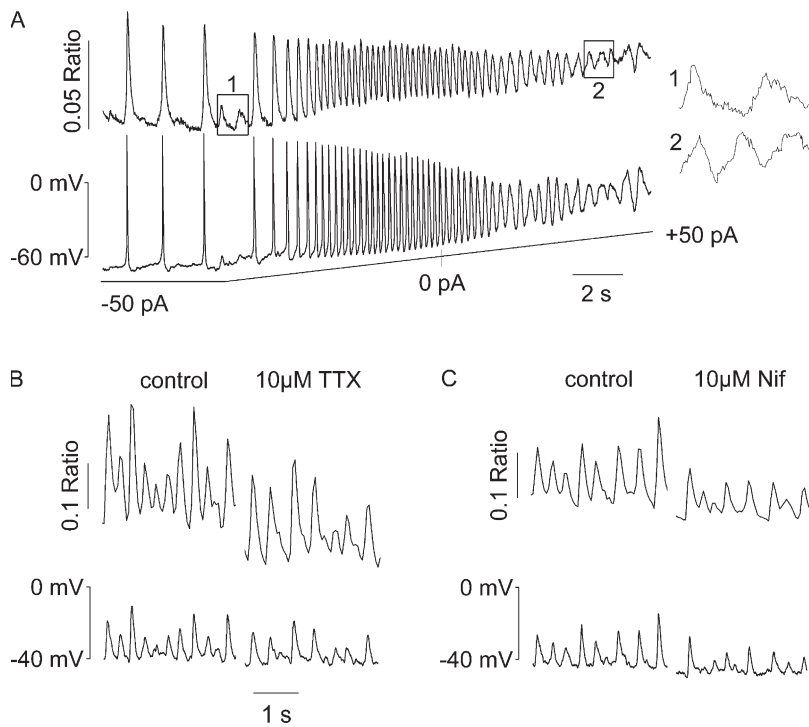
Figure 3. $[Ca^{2+}]_i$ and E_m oscillations persist after depolarization or blockade of excitatory inward currents. (A) Current injection (-50 pA) into a current-clamped cell results in an MDP of -70 mV and spontaneous APs with small subthreshold oscillations of $[Ca^{2+}]_i$ in between. Upon slowly changing the injected current from -50 pA to $+50$ pA the MDP increases and APs disappear. $[Ca^{2+}]_i$ oscillations are still present at depolarized potentials (-20 mV, insert 2) and of similar amplitude and frequency as at -70 mV (insert 1). (B and C) $[Ca^{2+}]_i$ and E_m oscillations persist after blocking either Na^+ (B; TTX 10 μM) or L-type Ca^{2+} channels (C, Nif: nifedipine 1–10 μM).

of the experiments shown in Fig. 1 B (Fig. S1), an example of $[Ca^{2+}]_i$ oscillations and APs in fresh dissociated embryonic cardiomyocytes (Fig. S2), and the movies of the experiments shown in Fig. 1 B, Fig. 2 A, and Fig. 7, B, E, and F (Videos 1–5).

RESULTS

Early Embryonic Cardiomyocytes Display Spontaneous $[Ca^{2+}]_i$ Oscillations and Contractions

Single cardiomyocytes isolated from early (E8.5–E10.5) embryonic murine hearts display robust contractions that persist for days. First, we characterized subcellular $[Ca^{2+}]_i$ signals potentially involved in the spontaneous electrical activity of early embryonic cardiomyocytes using high-speed 2-D confocal imaging (Fig. 1, A and B). Typically, large $[Ca^{2+}]_i$ transients ($\Delta F/F_0 = 2$–3, Fig. 1 B) were seen at regular intervals ($\sim$350 ms) in all parts of the cell except in the nuclear region where the $[Ca^{2+}]_i$ signals were smaller and had a delayed decay phase (black region and trace; Fig. 1, A and B). In the diastolic intervals between these transients, much smaller ($\Delta F/F_0 = 0.2$–0.4; Fig. 1 B, a–l) and regionally confined perinuclear $[Ca^{2+}]_i$ signals (blue, olive, green, yellow, orange, and red regions and traces; Fig. 1, A and B) were consistently observed. Such signals were found to be absent in the remaining cytoplasmic and nuclear regions (purple and black, respectively). These local increases of perinuclear $[Ca^{2+}]_i$ appeared to augment in number toward the end of diastolic intervals. As seen in the spatial analysis (Fig. 1, A and B; Video 1, available at http://www.jgp.org/cgi/content/full/jgp.200609575/DC1) and in the ratiometric images (Fig. S1), these small,

localized $[Ca^{2+}]_i$ signals were longer lasting ($\sim$50 ms) and more extended in space ($\sim$10 μm) as compared with the typical $[Ca^{2+}]_i$ sparks (5–20 ms, $\sim$1–2 μm) characteristic of adult cardiomyocytes (Cleemann et al., 1998; Woo et al., 2002, 2003).

To understand the mechanism(s) underlying the spontaneous $[Ca^{2+}]_i$ oscillations and contractions we combined whole cell patch-clamp and fast ratiometric $[Ca^{2+}]_i$ imaging methods. The large majority (63%, $n = 65$) of E8.5–10.5 embryonic cardiomyocytes displayed relatively depolarized maximum diastolic potentials (MDPs) of -33.2 ± 1.5 mV ($n = 41$) and regular oscillations of the membrane potential (E_m) at frequencies of 2.44 ± 0.15 Hz and spike amplitudes of 19.9 ± 1.8 mV ($n = 41$; Fig. 2 A, bottom). The changes in E_m were synchronized with oscillations of $[Ca^{2+}]_i$ (Fig. 2 A, top), which were unlike global Ca^{2+} increases spatially restricted and occurred in a repetitive wave-like pattern (see also Video 2). Optical movement detection analysis (Fig. 2 A, vertical lines) demonstrated that these small changes of $[Ca^{2+}]_i$ and E_m were accompanied by contractions (see also Video 2). Fast Fourier transformation of the data displayed in Fig. 2 A yielded for both $[Ca^{2+}]_i$ and E_m oscillations a distinct peak centered on a frequency of 3.75 Hz (Fig. 2 B), indicating their periodic nature. The width of the peak (± 0.2 Hz) indicates that the periodicity is typically maintained within $\sim \pm 5\%$. Besides the typical oscillatory pattern, 11% ($n = 65$) of cardiomyocytes displayed subthreshold E_m oscillations and aberrant APs (Fig. 2 C). Some cells (26%, $n = 65$) showed a more differentiated pattern of electrical activity including a more negative MDP of -60.6 ± 1.1 mV and larger spike amplitudes of 102.8 ± 2.3 mV occurring
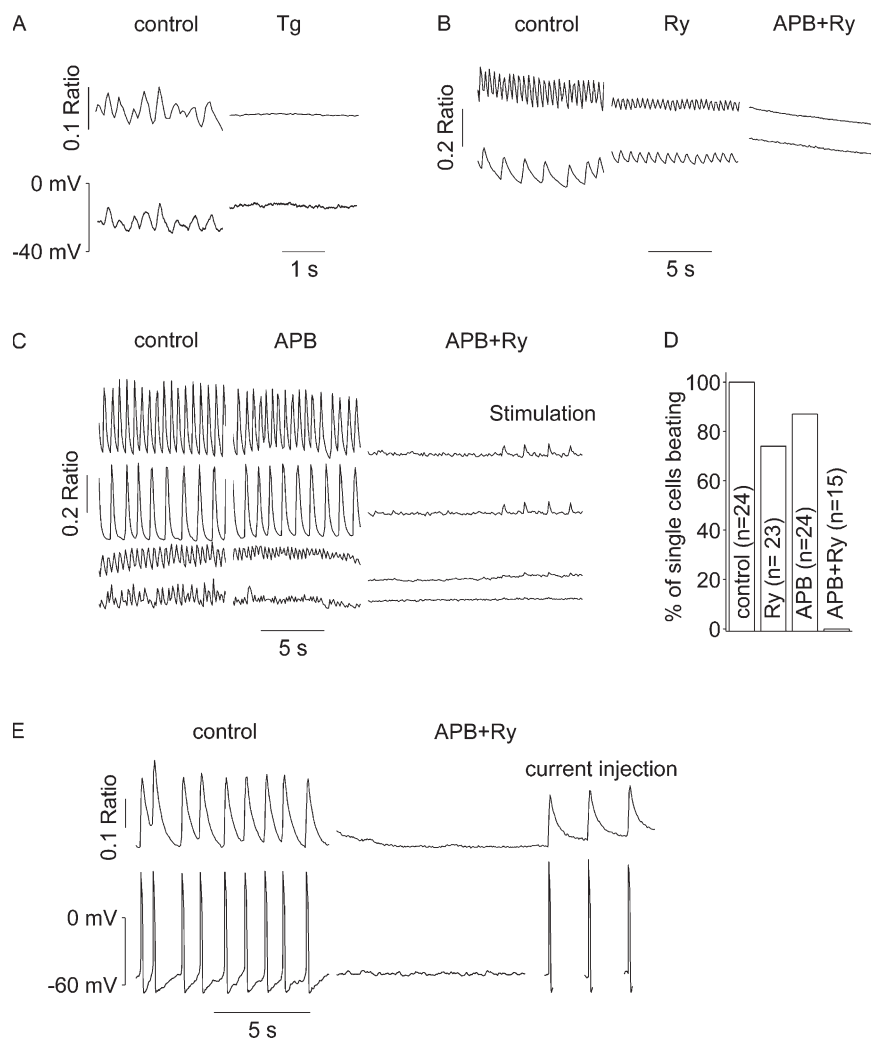
Figure 4. $[Ca^{2+}]_i$ oscillations originate from the SR. (A) Application of thapsigargin (2 μM) led to a complete halt of both $[Ca^{2+}]_i$ (top) and E_m (bottom) oscillations in patch-clamped cells. (B–E) Spontaneous activity ($[Ca^{2+}]_i$ oscillations or transients, left) in non (B and C) or perforated patch-clamped (E) and Fura-2-AM–loaded cardiomyocytes was unaltered in the majority of cells upon application of ryanodine (20 μM; B, middle) or 2-APB (100 μM; C, middle), whereas application of both blocked spontaneous activity in all cells (B, C, and E, right). The traces of individual cells (2 in B and 4 in C) were vertically shifted to be better visible. Cells with $[Ca^{2+}]_i$ transients could still be field stimulated (C, right, two top traces); APs could be evoked using brief (2-ms) current injections (E, right). (D) Analysis of the experiments shown in B and C.

at frequencies of 2.19 ± 0.17 Hz ($n = 17$; Fig. 2 D, left). However, block of the voltage-gated Na^+ channels with tetrodotoxin (TTX, 10 μM; Fig. 2 D, right) revealed even in this subset of cells oscillations of $[Ca^{2+}]_i$ and E_m similar to those of Fig. 2 A. The temporal relationship of Ca^{2+} and membrane signals was determined by plotting $[Ca^{2+}]_i$ versus E_m. In cells generating APs, this analysis yielded a hysteresis ($n = 4$; Fig. 2 E, left), implying the involvement of voltage-dependent ion channels and Ca^{2+} removal mechanisms (four phases indicated in the figure: depolarization and Ca^{2+} entry [a], repolarization with constant [b] and declining [c] $[Ca^{2+}]_i$, and E_m-independent Ca^{2+} extrusion [d]). After blocking Na^+ channels with TTX (Fig. 2 E, right) a 1:1 correlation in the E_m/Ca^{2+} loop became evident, indicating the difference from the all-or-nothing concept of APs. This pattern was observed in all cells ($n = 4$) displaying oscillations of $[Ca^{2+}]_i$ and E_m. Interestingly, the frequency of the oscillations upon TTX application (2.1 Hz) was similar to those of APs (2.4 Hz); this can also be seen in the Fourier analysis before (solid lines) and during application of TTX (dashed lines, Fig. 2 F).

Since cell culturing may result in changes of cell biological properties and ion channel expression we have performed control measurements in freshly isolated early embryonic (E9.5) cardiomyocytes within 6 h after dissociation. In analogy to our findings in cultured embryonic cardiomyocytes, we detected the characteristic $[Ca^{2+}]_i$ oscillations ($n = 12$) or $[Ca^{2+}]_i$ oscillations synchronous to oscillations of the E_m ($n = 4$, combining $[Ca^{2+}]_i$ and sharp electrode measurements; Fig. S2 A). In addition, AP-driven $[Ca^{2+}]_i$ transients were also observed and could be blocked by TTX, thereby revealing the underlying oscillations of $[Ca^{2+}]_i$ ($n = 21$) and E_m ($n = 2$, combining $[Ca^{2+}]_i$ and sharp electrode measurements; Fig. S2 B). Because earlier work in ES cell–derived cardiomyocytes was restricted to pacemaker-like cells (Mery et al., 2005), we determined whether the oscillations of $[Ca^{2+}]_i$ and E_m occurred only in a specific cardiomyocyte subtype. For this purpose we analyzed cells with APs where subthreshold oscillations of the E_m could be detected during the diastolic depolarization phase (Fig. 2 D, arrows). The cardiac subtype was identified based on shape and duration of the APs in the
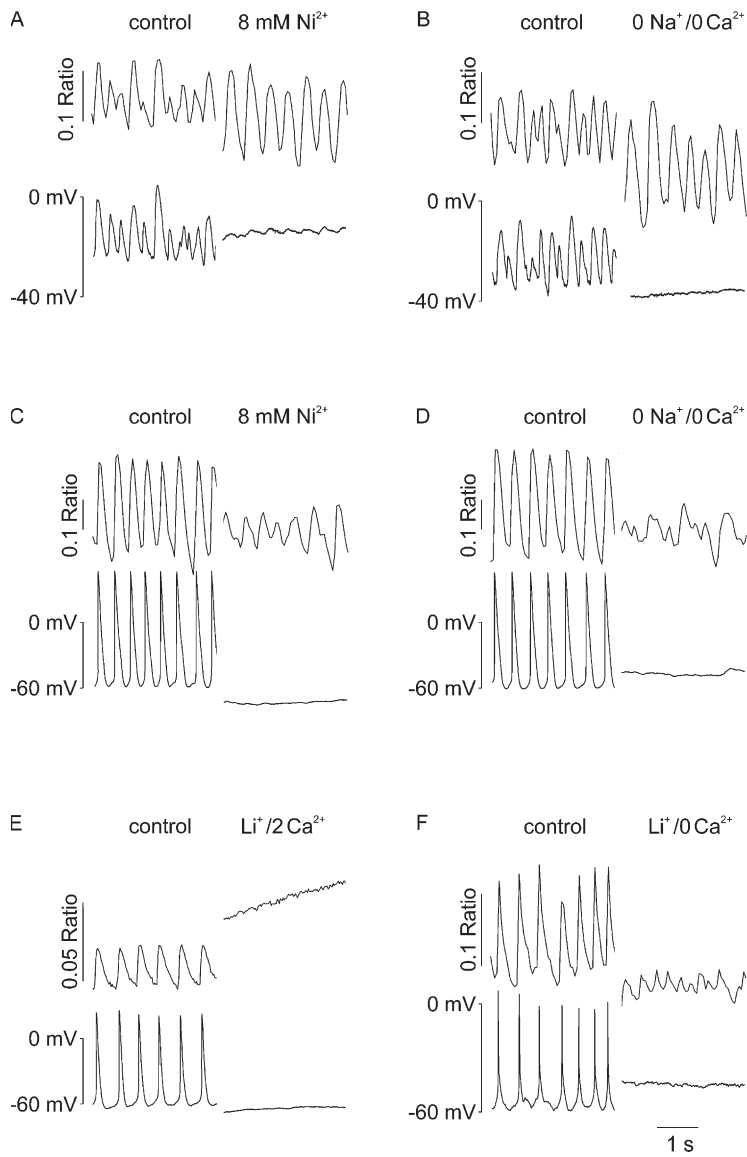
Figure 5. The NCX is responsible for E_m oscillations. Blockade of the NCX with Ni^{2+} (A, 8 mM) or replacement of extracellular Na^+ with choline (B) halted or significantly reduced the E_m oscillations (bottom) whereas the $[Ca^{2+}]_i$ oscillations (top) persisted. Application of Ni^{2+} (C, 8 mM) or replacement of Na^+ with choline (D) or Li^+ (F) in cells with APs blocked these completely and converted $[Ca^{2+}]_i$ transients into $[Ca^{2+}]_i$ oscillations of lower amplitude. Note that removal of Na^+ increased $[Ca^{2+}]_i$ (E) causing stop of $[Ca^{2+}]_i$ oscillations, therefore external Ca^{2+} also needed to be omitted (B, D, and F) to obtain persisting $[Ca^{2+}]_i$ oscillations; this is an additional proof for their intracellular nature. In F, $[Ca^{2+}]_i$ oscillations during Li^+ application occurred only in a small confined region that was used for the analysis; the remaining cell was silent.

current-clamp mode. This approach was established in an earlier study of our group where the combination of cardiac subtype-specific reporter gene expression and current clamp measurements in the ES cell system revealed characteristic features of the different cell types (Kolossov et al., 2005). We found that all three subtypes of early embryonic cardiomyocytes, pacemaker ($n = 4$), atrial ($n = 8$), and ventricular ($n = 5$)-like cells, displayed these typical oscillatory patterns.

Our data show that early embryonic cardiomyocytes spontaneously beat and contract even when triggered APs are absent. The contractions appear evoked by small $[Ca^{2+}]_i$ oscillations that are regionally confined.

Oscillations of $[Ca^{2+}]_i$ and E_m Persist after Membrane Depolarization or Blocking of Excitatory Ion Channels

To test the influence of the MDP on $[Ca^{2+}]_i$ oscillations, hyper- and depolarizing currents were injected into cardiomyocytes using ramp depolarizations in the current-clamp mode (Fig. 3 A). $[Ca^{2+}]_i$ transients and APs could be observed at negative MDPs; upon depolarization $[Ca^{2+}]_i$ and E_m oscillations persisted even though APs were suppressed (Fig. 3 A). The shape and amplitude of the spontaneous $[Ca^{2+}]_i$ oscillations (Fig. 3 A, insert 2) at depolarized MDPs were similar to those occurring in between the APs (Fig. 3 A, insert 1). This implies that the Ca^{2+} oscillations occur independently of the membrane potential and that the MDP determines if APs or $[Ca^{2+}]_i$ and E_m oscillations are present. In line with this, blockage of voltage-gated Na^+ ($n = 8$, Fig. 3 B) or L-type Ca^{2+} channels ($n = 7$, Fig. 3 C) with 10 µM TTX or nifedipine, respectively, had no significant effect on spontaneous oscillations of $[Ca^{2+}]_i$ and E_m in cells without APs, suggesting that activation of voltage-activated ion channels is not responsible for the generation of the subthreshold $[Ca^{2+}]_i$ oscillations.
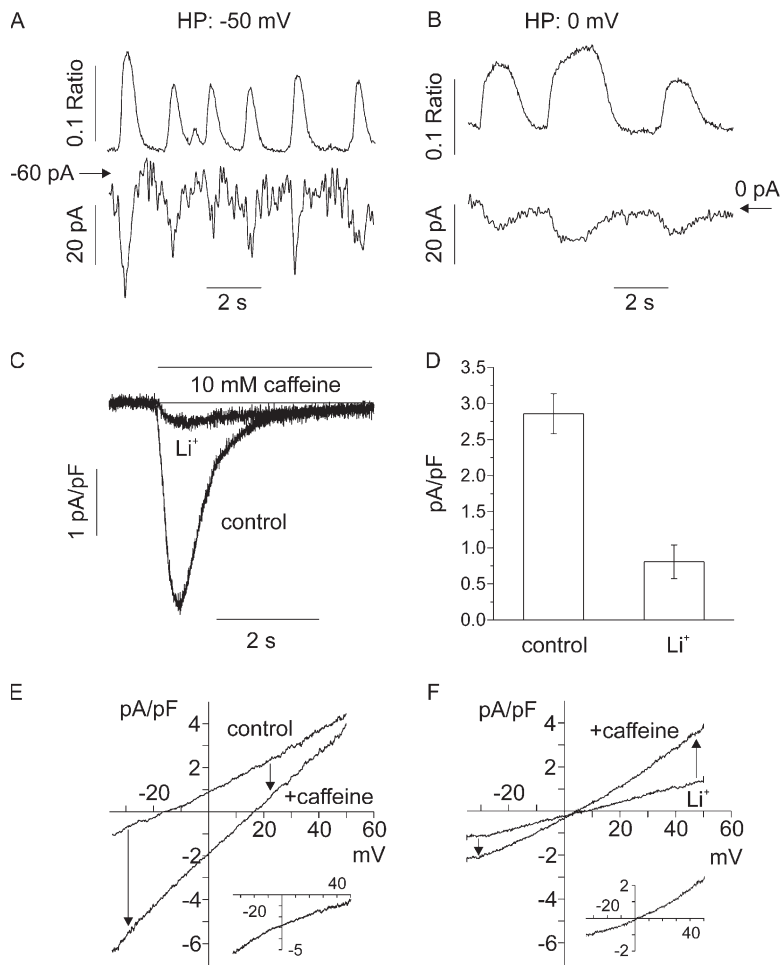
Figure 6. Biophysical characterization of the mechanism involved in translating $[Ca^{2+}]_i$ into E_m oscillations. (A and B) Spontaneous $[Ca^{2+}]_i$ oscillations (top) and simultaneous inward currents (bottom) in a voltage-clamped cardiomyocyte. The frequency of $[Ca^{2+}]_i$ oscillations and the amplitude of inward currents decreased at a holding potential of 0 mV (B) compared with −50 mV (A). (C) Application of caffeine evoked a large inward current that was significantly reduced when replacing Na^+ with Li^+ (holding potential −35 mV). (D) Statistical analysis of the caffeine evoked inward current in presence of Na^+ and Li^+. (E and F) Depolarizing voltage ramps (−35 mV to +50 mV, 250 ms, 1.4 Hz) applied before and in presence of caffeine revealed a linear inward current at potentials <+50 mV (E). When Na^+ was replaced by Li^+ the current reversed close to 0 mV and had a smaller amplitude (F). Inserts show the subtracted Ca^{2+}-activated currents.

Oscillations of $[Ca^{2+}]_i$ Originate from the SR and Are Accompanied by Changes of E_m

To identify the origin of the $[Ca^{2+}]_i$ oscillations, thapsigargin (2 μM; Fig. 4 A), an inhibitor of the SR-Ca^{2+}-ATPase, was used to deplete the intracellular Ca^{2+} stores; this stopped the oscillations of $[Ca^{2+}]_i$ and of E_m even though resting $[Ca^{2+}]_i$ changed relatively little. $[Ca^{2+}]_i$ imaging experiments in Fura-2-AM–loaded and spontaneously beating single cardiomyocytes showed that ryanodine (20 μM) blocked spontaneous $[Ca^{2+}]_i$ transients or oscillations in only 26% of cardiomyocytes ($n = 23$; Fig. 4 B, middle) while the IP_3 receptor (IP_3R) blocker 2-APB (100 μM) was effective in only 13% of cells ($n = 24$; Fig. 4 C, middle). The combined use of ryanodine and 2-APB completely stopped spontaneous activity ($[Ca^{2+}]_i$ transients or oscillations) in all cardiomyocytes tested ($n = 15$; Fig. 4, B–D, right). In addition, the excitability of these cells remained intact as electrical field stimulation induced $[Ca^{2+}]_i$ spiking (Fig. 4 C, right). This was further corroborated by the combined use of Ca^{2+} imaging and perforated patch clamp technique (see Materials and Methods). We noticed a complete halt of APs and $[Ca^{2+}]_i$ transients upon application of ryanodine and 2-APB, while brief (2-ms) current injections could still induce APs and corresponding $[Ca^{2+}]_i$ transients ($n = 3$; Fig. 4 E, right). Thus, intracellular RyR and IP_3R underlie the $[Ca^{2+}]_i$ oscillations and spontaneous beating.

We next determined the origin of the E_m oscillations by blocking all transmembrane Ca^{2+} fluxes using 8 mM Ni^{2+} (Fig. 5 A). This left the $[Ca^{2+}]_i$ oscillations unaltered whereas oscillations of E_m were completely ($n = 8$) or almost completely ($n = 11$) abolished. The E_m but not the $[Ca^{2+}]_i$ oscillations could also be rapidly and completely suppressed by removal of extracellular Na^+ and Ca^{2+} ($n = 14$; Fig. 5 B). Similar results were obtained in cells with APs and $[Ca^{2+}]_i$ transients where either application of 8 mM Ni^{2+} ($n = 7$; Fig. 5 C), removal of Na^+/Ca^{2+} ($n = 4$; Fig. 5 D), or isomolar replacement of Na^+ by Li^+ ($n = 4$; Fig. 5 F) abolished changes of the E_m and converted $[Ca^{2+}]_i$ transients into subthreshold $[Ca^{2+}]_i$ oscillations. Since removal of extracellular Na^+ leads to elevation of $[Ca^{2+}]_i$ and consequent block of $[Ca^{2+}]_i$ oscillations ($n = 9$; Fig. 5 E), external Ca^{2+} was also removed. Under these conditions E_m oscillations (Fig. 5 B) and AP generation stopped (Fig. 5, D and F), whereas $[Ca^{2+}]_i$ oscillations persisted, suggesting that these originate from intracellular stores. It should be
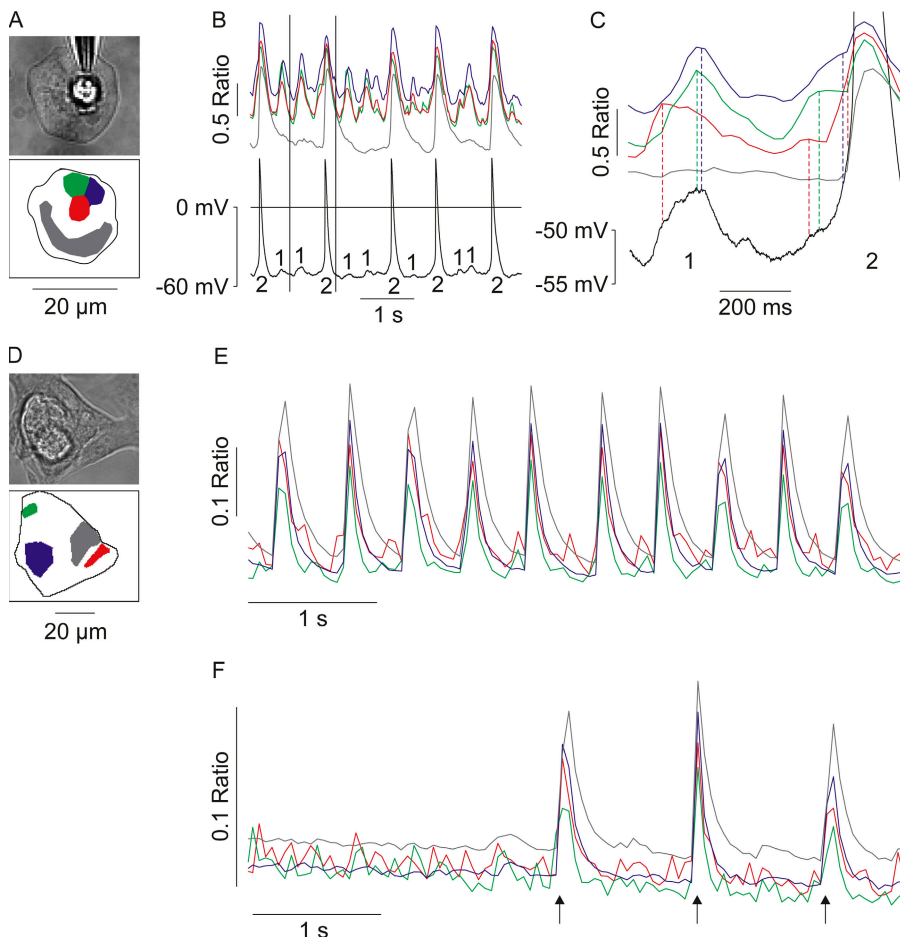
Figure 7. $[Ca^{2+}]_i$ oscillations are local events in embryonic cardiomyocytes whereas APs synchronize the individual cells. (A–C) Transmission image (A, top) and schematic representation (A, bottom) of a spontaneously beating heart cell. Simultaneous recording of E_m (black trace) and $[Ca^{2+}]_i$ from four different areas of the cell (red, green, blue, and gray traces) revealed that the $[Ca^{2+}]_i$ oscillations occurred synchronously with subthreshold E_m oscillations (labeled by 1). These were confined to a small area in the cell (red, green, and blue regions), occurred periodically, and were synchronized but with a slight delay in the three regions indicating the wave-like pattern of $[Ca^{2+}]_i$ oscillations (see also Video 3). In the remaining part of the cell (gray region) no changes of $[Ca^{2+}]_i$ were detected except during APs (B, labeled by 2). Higher time resolution (C) revealed that the E_m was influenced by the spatial summation of $[Ca^{2+}]_i$ in all regions. Dashed lines highlight peak $[Ca^{2+}]_i$ of the subcellular regions and their depolarizing action on the E_m. When $[Ca^{2+}]_i$ is highest in all regions, the threshold potential is reached, evoking an AP. (D–F) $[Ca^{2+}]_i$ imaging of a spontaneously beating, multicellular cluster of embryonic cardiomyocytes loaded with Fura-2-AM. (D) Transmission picture (top) and schematic representation (bottom). (E) Two subcellular regions (red and green regions and traces) displayed individual $[Ca^{2+}]_i$ oscillations between the $[Ca^{2+}]_i$ transients; these were synchronized in the whole cell cluster (blue and gray regions and traces). (F) Application of 10 μM TTX blocked the global synchronized $[Ca^{2+}]_i$ transients, whereas the two subcellular oscillators remained unperturbed. Electrical field stimulation (indicated by arrows) still evoked synchronized $[Ca^{2+}]_i$ transients.

noted that the frequency of $[Ca^{2+}]_i$ oscillations uncovered in the presence of Ni^{2+} (2.2 Hz; Fig. 5 C) was similar to the frequency of APs (2.6 Hz) before the application of Ni^{2+}. These data suggest that oscillations of $[Ca^{2+}]_i$ originate from the SR and trigger the oscillations of the E_m most likely via the activation of the NCX.

Activation of NCX Mediated the E_m Oscillations

To further prove that $[Ca^{2+}]_i$ oscillations are independent of a possible E_m oscillator we next measured $[Ca^{2+}]_i$ while holding the E_m constant in the voltage clamp mode. $[Ca^{2+}]_i$ oscillations and accompanying inward currents persisted at holding potentials of -50 (Fig. 6 A) and 0 mV (Fig. 6 B), but with reduced amplitude at 0 mV. To better identify the nature of the Ca^{2+}-activated current we released Ca^{2+} from the SR with caffeine (10 mM) in the voltage clamp mode. This results in inward currents at a holding potential of -35 mV in normal extracellular solution and upon isomolar replacement of Na^+ by the NCX-impermanent ion Li^+. Fig. 6 C shows that caffeine activated a large inward current of 2.86 ± 0.28 pA/pF

($n = 9$; Fig. 6 D), which was strongly reduced by $71.7 \pm 6.5\%$ to 0.81 ± 0.23 pA/pF ($P < 0.001$, paired t test, $n = 9$; Fig. 6 D) in presence of Li^+. The Li^+-sensitive and insensitive current components were further characterized by applying depolarizing voltage ramps (-35 to $+50$ mV, 250 ms) prior and during caffeine application. In normal Na^+-containing solution, the caffeine-evoked current remained in the inward direction as expected for NCX ($n = 4$; Fig. 6 E). In the presence of Li^+, caffeine still induced a small current that reversed close to 0 mV ($+6.8 \pm 1.9$ mV, $n = 8$; Fig. 6 F).

Localization of $[Ca^{2+}]_i$ Oscillations, Generation of APs, and Synchronization between the Individual Heart Cells

We next analyzed the subcellular spatial localization of the $[Ca^{2+}]_i$ oscillator(s) as well as of the AP-triggered $[Ca^{2+}]_i$ transients. Spontaneous $[Ca^{2+}]_i$ oscillations were spatially restricted to a specific site of the cell (Fig. 7, A and B, red, green, and blue regions, labeled with 1), whereas a global rise in $[Ca^{2+}]_i$ only occurred during APs (Fig. 7, A and B, gray region, labeled with 2; see

also Video 3). A delay of the $[Ca^{2+}]_i$ rise can be seen in between the synchronous individual oscillatory regions (Fig. 7 C, red, green, and blue lines), indicating the wave-like nature (see also Video 3) of the propagating $[Ca^{2+}]_i$ oscillation. The amplitude of the $[Ca^{2+}]_i$ oscillations induced subthreshold changes of the E_m independent of their location (see peaks indicated by dashed lines in Fig. 7 C).

Although early embryonic heart cells are individual $[Ca^{2+}]_i$ oscillators, the embryonic heart displays right from the beginning synchronized contractions (Kamino, 1991). To reconcile these apparently contrasting findings we performed experiments on multicellular preparations (incomplete dissociation) and analyzed the crosstalk between cardiomyocytes. We identified individual pacemaking cells displaying $[Ca^{2+}]_i$ oscillations (Fig. 7, D and E, red and green cells and traces), however, these were not transferred to the other cardiomyocytes in the syncytium (Fig. 7, D and E, gray and blue cells and traces; Video 4). By contrast, the global $[Ca^{2+}]_i$ events (APs) were transmitted to all myocytes within the same cluster and lead to synchronous contractions. Blockage of the APs with 10 µM TTX inhibited the global, synchronized $[Ca^{2+}]_i$ transients and contractions whereas the intracellular oscillators (red and green cells and traces) remained unperturbed (Fig. 7 F; Video 5). Importantly, TTX only had effect on the excitation but not on the excitability of myocytes, since electrical stimulation still evoked synchronized $[Ca^{2+}]_i$ transients and contractions (Fig. 7 F, right; Video 5). Hence, electrical and mechanic synchronization within the embryonic heart is achieved through $[Ca^{2+}]_i$ oscillation–evoked APs.

DISCUSSION

The mechanisms underlying the initiation of the heart beat are still poorly understood. Here we show that early embryonic heart cells display small, but stable, $[Ca^{2+}]_i$ oscillations that can evoke contractions. Our biophysical and pharmacological evidence suggests that such oscillations can activate small depolarizations of the E_m via the NCX. Such depolarizations, when reaching threshold potential, give rise to APs that synchronize the activity of individual heart cells. The $[Ca^{2+}]_i$ oscillations are not restricted to cardiac subtypes but can be detected in pacemaker-, atrial-, and ventricular-like early embryonic cardiomyocytes. Thus, although the early embryonic heart consists of individual $[Ca^{2+}]_i$ oscillators, APs appear to synchronize contractions and the coordinated pumping of blood.

The finding that $[Ca^{2+}]_i$ oscillations drive spontaneous contractions without APs in early embryonic heart cells is in agreement with our observations in ES cell−derived cardiomyocytes, where persistence of spontaneous beating in high extracellular K^+ solution was reported (Viatchenko-Karpinski et al., 1999). However, these studies were restricted to ES cell–derived cardiomyocytes and could neither exclude $[Ca^{2+}]_i$ overloading secondary to high K^+ depolarization nor resolve the underlying mechanism. Our pharmacological data suggest that $[Ca^{2+}]_i$ oscillations originate from the SR and are likely critical for pacemaking, as oscillations of both $[Ca^{2+}]_i$ and E_m halt after suppression of Ca^{2+} release from intracellular stores (Fig. 4). NCX is most likely the key membrane protein to convert $[Ca^{2+}]_i$ oscillations into changes of E_m (Figs. 5 and 6). This is in agreement with the proposed role of the NCX in the early embryonic heart where it is strongly up-regulated (Reppel et al., 2007) and where its deletion leads to loss of spontaneous beating in the NCX-deficient embryos despite preserved excitability (Koushik et al., 2001).

Besides NCX, we have also found evidence for the involvement, although to a lesser degree, of a Ca^{2+}-activated nonselective cation current (Fig. 6, C, D, and F). Its molecular identity is unknown, but TRPM4 is one likely candidate as it is Ca^{2+} activated, Ca^{2+} impermeable, and known to be expressed in the adult heart (Nilius et al., 2003). Ca^{2+}-activated Cl^- currents were found to not play a significant role in this process, as inward currents were observed at an HP of -35 mV, which is close the reversal potential of Cl^- (-28 mV).

$[Ca^{2+}]_i$ oscillations may be also responsible for the unexpected automaticity observed in E9.5 embryonic hearts of mice deficient in HCN4 (Seisenberger et al., 2000) and Cav1.2 (Stieber et al., 2003) channels.

The generation of APs is critical for intracellular synchronization of the $[Ca^{2+}]_i$ throughout the cell (Fig. 7, B and C) and for intercellular synchronization of a cluster of cells within the electrical syncytium (Fig. 7 E). Interestingly, we find that the majority of the cells in culture have spontaneous $[Ca^{2+}]_i$ oscillations without APs. At this point we do not know, whether these cells are typical of the embryonic heart before the initiation of the heart beat and/or these cells exist also in vivo in the embryonic heart at later stages of development. Nevertheless, these cells (Fig. 2 A) as well as those with intermittent (Fig. 2 C; Fig. 7, A–C) or continuous APs (Fig. 2 D) are characterized by the presence of $[Ca^{2+}]_i$ oscillations. As soon as APs are blocked, oscillations of the E_m are observed and this is a property of freshly isolated (Fig. S2 B) as well as cultured early embryonic cardiomyocytes (Fig. 2 D; Fig. 5, C, D, and F). The physiological relevance of the $[Ca^{2+}]_i$ oscillations at the embryonic stage will require the combined use of novel genetic Ca^{2+} indicators and high speed Ca^{2+} imaging in vivo.

The analysis of our data indicate that the APs do not have a major influence on the occurrence of $[Ca^{2+}]_i$ oscillations as (a) conversion of APs into oscillations with TTX (Fig. 2, D and F) or with Ni^{2+} (Fig. 5 C) has only little or no effect on the frequency of $[Ca^{2+}]_i$ oscillations and (b) cells displaying $[Ca^{2+}]_i$ oscillations only have similar frequencies to those generating APs.

$[Ca^{2+}]_i$ oscillations occur periodically and in a wave-like manner (Fig. 2, A and B; Video 2; Fig. 7, B and C; Video 3). These are spatially confined within a cell (see red, green, and blue region and traces at $[Ca^{2+}]_i$ oscillations labeled 1 in Fig. 7, B and C; see also Video 3). This suggests their independence of E_m signals since, assuming homogeneous channel distribution on the surface membrane, an E_m oscillator would produce a uniform and global rise in $[Ca^{2+}]_i$ similar as in the case of APs (see APs labeled 2 in Fig. 7, B and C). In contrast to epifluorescence recordings that present periodic propagating $[Ca^{2+}]_i$ oscillations, confocal imaging (Fig. 1 B) suggests spatially independent Ca^{2+} release sites in different regions of the cell. We presume that this apparent discrepancy is related to differences in the two recording techniques as epifluorescence imaging integrates the fluorescence of the whole cell while confocal imaging is confined to a much thinner optical plane and thereby less suited to record spatially propagating Ca^{2+} waves. Nevertheless, confocal recording shows that local Ca^{2+} releases found in embryonic heart muscle cells are larger in size and duration from the classical $[Ca^{2+}]_i$ sparks reported in adult cardiomyocytes.

Although the mechanisms underlying the regular oscillations still remain unclear, a recent review on adult sino-atrial node pacemaker cells is in accordance with our findings and suggests that local Ca^{2+} release "generated by free running SR is roughly periodic" (Maltsev et al., 2006). The concept of a "free running" SR is consistent with the finding that early embryonic cardiomyocytes yet to have T-tubules, and thus functional interaction with the surface Ca^{2+} channel and CICR contributes little to AP-induced Ca^{2+} transients (Bloch, W., personal communication; Sasse, P., M. Reppel, J. Hescheler, and B.K. Fleischmann. 2005. *Biophys. J.* 88:321A–322A). We therefore propose besides the earlier discussed physical/functional disconnection (Maltsev et al., 2006) a "developmental" disconnection of the SR from AP entrainment in early embryonic cardiomyocytes. Computational models propose RyR-dependent periodic $[Ca^{2+}]_i$ oscillations where spontaneous (stochastic) SR Ca^{2+} release is determined by SR Ca^{2+} content and propagated via CICR (Goldbeter et al., 1990; Keizer and Levine, 1996), resulting in periodic $[Ca^{2+}]_i$ waves. Alternative models of IP$_3$-dependent periodic $[Ca^{2+}]_i$ oscillations exist where (stochastic) IP$_3$R are modulated by $[Ca^{2+}]_i$ in a biphasic manner (Atri et al., 1993). Our data indicate that both RyR- and IP$_3$R-gated mechanisms coexist in early embryonic cardiomyocytes, as only the combined use of RyR and IP$_3$R blockers was effective in stopping spontaneous beating (Fig. 4, B–E). This is in agreement with earlier reports where RyR2-deficient mice (Takeshima et al., 1998) were found to initiate spontaneous beating at the early developmental stage and RyR (−/−) ES cell–derived cardiomyocytes beat (Yang et al., 2002) but with a reduced frequency compared with wild-type cells. We could not detect exclusively IP$_3$R-driven $[Ca^{2+}]_i$ oscillations, as reported for ES cell–derived pacemaker like cardiomyocytes (Mery et al., 2005).

Oscillations in general are well known and a widespread biological phenomena. Oscillatory patterns and waves are considered rudimentary, but thermodynamically stable and therefore particularly well suited for primitive biological systems. $[Ca^{2+}]_i$ oscillations are intrinsically associated with early stages of life since conception and fertilization critically depend on these IP$_3$-dependent mechanisms (Dumollard et al., 2002). Specific patterns of $[Ca^{2+}]_i$ cycling appear to play a key role for gene expression and development as illustrated in the immunological system (Dolmetsch et al., 1997; Healy et al., 1997). Furthermore, changes in $[Ca^{2+}]_i$ homeostasis appear to cause defective myocyte development and myofibrillogenesis in the ES cell system (Li et al., 2002). This is consistent with the finding that metabolic poisoning caused abolishment of $[Ca^{2+}]_i$ oscillations and a halt of cardiac differentiation in the ES cell system and that this effect could be rescued by the Ca^{2+} ionophore ionomycin (Spitkovsky et al., 2004).

It is well known that E_m and $[Ca^{2+}]_i$ cycling are bidirectional in terminal differentiated cardiomyocytes. We cannot entirely exclude the possible involvement of an E_m-dependent oscillator driving or modulating the intracellular $[Ca^{2+}]_i$ oscillator. All the pharmacological interventions to block SR Ca^{2+} release could also affect the E_m oscillator directly or secondary to blocking the $[Ca^{2+}]_i$ oscillations. This could potentially alter the properties of the voltage-driven mechanism by pushing it out of the oscillatory regime. Nevertheless, several of our experimental findings are against E_m being the prime oscillator in early embryonic cardiomyocytes: (a) depolarization of the membrane (Fig. 3 A, inserts) or inhibition of the classic voltage-dependent ion channels (Fig. 3, B and C) has little effect on the frequency of $[Ca^{2+}]_i$ oscillations; (b) all pharmacological interventions that block NCX (Ni^{2+}, 0Na$^+$, Li$^+$; Fig. 5) stop the E_m signals (APs or oscillations) and $[Ca^{2+}]_i$ transients, whereas $[Ca^{2+}]_i$ oscillations continue to persist at similar frequencies and even similar amplitude in the cells without APs; (c) inhibition of the SR release with ryanodine and APB blocked both spontaneous $[Ca^{2+}]_i$ oscillations and AP formation; (d) $[Ca^{2+}]_i$ oscillations are spatially localized events and occur in a wave-like manner (Fig. 2, A and B; Video 2; Fig. 7, B and C; Video 3); and (e) $[Ca^{2+}]_i$ oscillations persist at fixed E_m in the voltage clamp mode (Fig. 6, A and B).

The fact that the initiation of spontaneous contractions during embryonic development is due to $[Ca^{2+}]_i$ oscillations rather than membrane-delimited events may have even wider implications as there is increasing evidence that spontaneous Ca^{2+} release contributes to

the diastolic depolarization phase of adult sino-atrial node (Maltsev et al., 2004, 2006; Vinogradova et al., 2004) and atrial cells (Blatter et al., 2003). In contrast to the embryonic cells, in adult pacemaker cells E_m determines the spontaneous activity whereas $[Ca^{2+}]_i$ release and NCX activation appear to augment the terminal depolarization rate, thereby modulating the frequency of pacing (Maltsev et al., 2004, 2006; Vinogradova et al., 2004). It is well known that terminally differentiated cardiomyocytes recapitulate embryonic genes and phenotypes under pathophysiological conditions. In fact spontaneous $[Ca^{2+}]_i$ oscillations inducing delayed afterdepolarizations (DADs) have been reported in acutely and chronically lesioned adult cardiomyocytes of dogs and humans (Verkerk et al., 2001; Janse, 2004; Katra and Laurita, 2005). These DADs appear to be evoked by activation of the NCX (Schlotthauer and Bers, 2000; Verkerk et al., 2001) and are thought to potentially evoke single focus-induced life-threatening arrhythmias (Clusin, 2003; Janse, 2004; Rubart and Zipes, 2005; Lehnart et al., 2006).

A better mechanistic understanding of fundamental physiological processes in the embryonic heart may therefore provide in the future novel clues for pharmacological interventions in the prevention and treatment of arrhythmias.

REFERENCES

Abi-Gerges, N., G.J. Ji, Z.J. Lu, R. Fischmeister, J. Hescheler, and B.K. Fleischmann. 2000. Functional expression and regulation of the hyperpolarization activated non-selective cation current in embryonic stem cell-derived cardiomyocytes. *J. Physiol.* 523:377–389.

Adachi-Akahane, S., L. Cleemann, and M. Morad. 1996. Cross-signaling between L-type Ca^{2+} channels and ryanodine receptors in rat ventricular myocytes. *J. Gen. Physiol.* 108:435–454.

Atri, A., J. Amundson, D. Clapham, and J. Sneyd. 1993. A single-pool model for intracellular calcium oscillations and waves in the *Xenopus laevis* oocyte. *Biophys. J.* 65:1727–1739.

Baruscotti, M., and D. DiFrancesco. 2004. Pacemaker channels. *Ann. N. Y. Acad. Sci.* 1015:111–121.

Blatter, L.A., J. Kockskamper, K.A. Sheehan, A.V. Zima, J. Huser, and S.L. Lipsius. 2003. Local calcium gradients during excitation-contraction coupling and alternans in atrial myocytes. *J. Physiol.* 546:19–31.

Bony, C., S. Roche, U. Shuichi, T. Sasaki, M.A. Crackower, J. Penninger, H. Mano, and M. Puceat. 2001. A specific role of phosphatidylinositol 3-kinase gamma. A regulation of autonomic Ca^{2+} oscillations in cardiac cells. *J. Cell Biol.* 152:717–728.

Cleemann, L., W. Wang, and M. Morad. 1998. Two-dimensional confocal images of organization, density, and gating of focal Ca^{2+} release sites in rat cardiac myocytes. *Proc. Natl. Acad. Sci. USA.* 95:10984–10989.

Clusin, W.T. 2003. Calcium and cardiac arrhythmias: DADs, EADs, and alternans. *Crit. Rev. Clin. Lab. Sci.* 40:337–375.

Dolmetsch, R.E., R.S. Lewis, C.C. Goodnow, and J.I. Healy. 1997. Differential activation of transcription factors induced by Ca^{2+} response amplitude and duration. *Nature.* 386:855–858.

Dumollard, R., J. Carroll, G. Dupont, and C. Sardet. 2002. Calcium wave pacemakers in eggs. *J. Cell Sci.* 115:3557–3564.

Fabiato, A. 1983. Calcium-induced release of calcium from the cardiac sarcoplasmic reticulum. *Am. J. Physiol.* 245:C1–14.

Fleischmann, B.K., Y. Duan, Y. Fan, T. Schoneberg, A. Ehlich, N. Lenka, S. Viatchenko-Karpinski, L. Pott, J. Hescheler, and B. Fakler. 2004. Differential subunit composition of the G protein-activated inward-rectifier potassium channel during cardiac development. *J. Clin. Invest.* 114:994–1001.

Goldbeter, A., G. Dupont, and M.J. Berridge. 1990. Minimal model for signal-induced Ca^{2+} oscillations and for their frequency encoding through protein phosphorylation. *Proc. Natl. Acad. Sci. USA.* 87:1461–1465.

Healy, J.I., R.E. Dolmetsch, L.A. Timmerman, J.G. Cyster, M.L. Thomas, G.R. Crabtree, R.S. Lewis, and C.C. Goodnow. 1997. Different nuclear signals are activated by the b cell receptor during positive versus negative signaling. *Immunity.* 6:419–428.

Herr, C., N. Smyth, S. Ullrich, F. Yun, P. Sasse, J. Hescheler, B. Fleischmann, K. Lasek, K. Brixius, R.H. Schwinger, et al. 2001. Loss of annexin A7 leads to alterations in frequency-induced shortening of isolated murine cardiomyocytes. *Mol. Cell. Biol.* 21:4119–4128.

Janse, M.J. 2004. Electrophysiological changes in heart failure and their relationship to arrhythmogenesis. *Cardiovasc. Res.* 61:208–217.

Kamino, K. 1991. Optical approaches to ontogeny of electrical activity and related functional organization during early heart development. *Physiol. Rev.* 71:53–91.

Katra, R.P., and K.R. Laurita. 2005. Cellular mechanism of calcium-mediated triggered activity in the heart. *Circ. Res.* 96:535–542.

Keizer, J., and L. Levine. 1996. Ryanodine receptor adaptation and Ca^{2+}-induced Ca^{2+} release-dependent Ca^{2+} oscillations. *Biophys. J.* 71:3477–3487.

Kolossov, E., B.K. Fleischmann, Q. Liu, W. Bloch, S. Viatchenko-Karpinski, O. Manzke, G.J. Ji, H. Bohlen, K. Addicks, and J. Hescheler. 1998. Functional characteristics of ES cell-derived cardiac precursor cells identified by tissue-specific expression of the green fluorescent protein. *J. Cell Biol.* 143:2045–2056.

Kolossov, E., Z. Lu, I. Drobinskaya, N. Gassanov, Y. Duan, H. Sauer, O. Manzke, W. Bloch, H. Bohlen, J. Hescheler, and B.K. Fleischmann. 2005. Identification and characterization of embryonic stem cell-derived pacemaker and atrial cardiomyocytes. *FASEB J.* 19:577–579.

Koushik, S.V., J. Wang, R. Rogers, D. Moskophidis, N.A. Lambert, T.L. Creazzo, and S.J. Conway. 2001. Targeted inactivation of the sodium-calcium exchanger (Ncx1) results in the lack of a heartbeat and abnormal myofibrillar organization. *FASEB J.* 15:1209–1211.

Lehnart, S.E., C. Terrenoire, S. Reiken, X.H. Wehrens, L.S. Song, E.J. Tillman, S. Mancarella, J. Coromilas, W.J. Lederer, R.S. Kass, and A.R. Marks. 2006. Stabilization of cardiac ryanodine receptor prevents intracellular calcium leak and arrhythmias. *Proc. Natl. Acad. Sci. USA.* 103:7906–7910.

Li, J., M. Puceat, C. Perez-Terzic, A. Mery, K. Nakamura, M. Michalak, K.H. Krause, and M.E. Jaconi. 2002. Calreticulin reveals a critical Ca^{2+} checkpoint in cardiac myofibrillogenesis. *J. Cell Biol.* 158:103–113.

Maltsev, V.A., T.M. Vinogradova, K.Y. Bogdanov, E.G. Lakatta, and M.D. Stern. 2004. Diastolic calcium release controls the beating

rate of rabbit sinoatrial node cells: numerical modeling of the coupling process. *Biophys. J.* 86:2596–2605.

Maltsev, V.A., T.M. Vinogradova, and E.G. Lakatta. 2006. The emergence of a general theory of the initiation and strength of the heartbeat. *J. Pharmacol. Sci.* 100:338–369.

Maltsev, V.A., A.M. Wobus, J. Rohwedel, M. Bader, and J. Hescheler. 1994. Cardiomyocytes differentiated in vitro from embryonic stem cells developmentally express cardiac-specific genes and ionic currents. *Circ. Res.* 75:233–244.

Mery, A., F. Aimond, C. Menard, K. Mikoshiba, M. Michalak, and M. Puceat. 2005. Initiation of embryonic cardiac pacemaker activity by inositol 1,4,5-trisphosphate-dependent calcium signaling. *Mol. Biol. Cell.* 16:2414–2423.

Nilius, B., J. Prenen, G. Droogmans, T. Voets, R. Vennekens, M. Freichel, U. Wissenbach, and V. Flockerzi. 2003. Voltage dependence of the Ca^{2+}-activated cation channel TRPM4. *J. Biol. Chem.* 278:30813–30820.

Reppel, M., P. Sasse, D. Malan, F. Nguemo, H. Reuter, W. Bloch, J. Hescheler, and B.K. Fleischmann. 2007. Functional expression of the Na^+/Ca^{2+} exchanger in the embryonic mouse heart. *J. Mol. Cell. Cardiol.* 42:121–132.

Rubart, M., and D.P. Zipes. 2005. Mechanisms of sudden cardiac death. *J. Clin. Invest.* 115:2305–2315.

Schlotthauer, K., and D.M. Bers. 2000. Sarcoplasmic reticulum Ca^{2+} release causes myocyte depolarization. Underlying mechanism and threshold for triggered action potentials. *Circ. Res.* 87:774–780.

Schram, G., M. Pourrier, P. Melnyk, and S. Nattel. 2002. Differential distribution of cardiac ion channel expression as a basis for regional specialization in electrical function. *Circ. Res.* 90:939–950.

Seisenberger, C., V. Specht, A. Welling, J. Platzer, A. Pfeifer, S. Kuhbandner, J. Striessnig, N. Klugbauer, R. Feil, and F. Hofmann. 2000. Functional embryonic cardiomyocytes after disruption of the L-type alpha 1C (Cav1.2) calcium channel gene in the mouse. *J. Biol. Chem.* 275:39193–39199.

Shih, H.T. 1994. Anatomy of the action potential in the heart. *Tex. Heart Inst. J.* 21:30–41.

Spitkovsky, D., P. Sasse, E. Kolossov, C. Bottinger, B.K. Fleischmann, J. Hescheler, and R.J. Wiesner. 2004. Activity of complex III of the mitochondrial electron transport chain is essential for early heart muscle cell differentiation. *FASEB J.* 18:1300–1302.

Stieber, J., S. Herrmann, S. Feil, J. Loster, R. Feil, M. Biel, F. Hofmann, and A. Ludwig. 2003. The hyperpolarization-activated channel HCN4 is required for the generation of pacemaker action potentials in the embryonic heart. *Proc. Natl. Acad. Sci. USA.* 100:15235–15240.

Takeshima, H., S. Komazaki, K. Hirose, M. Nishi, T. Noda, and M. Iino. 1998. Embryonic lethality and abnormal cardiac myocytes in mice lacking ryanodine receptor type 2. *EMBO J.* 17:3309–3316.

Verkerk, A.O., M.W. Veldkamp, A. Baartscheer, C.A. Schumacher, C. Klopping, A.C. van Ginneken, and J.H. Ravesloot. 2001. Ionic mechanism of delayed afterdepolarizations in ventricular cells isolated from human end-stage failing hearts. *Circulation.* 104:2728–2733.

Viatchenko-Karpinski, S., B.K. Fleischmann, Q. Liu, H. Sauer, O. Gryshchenko, G.J. Ji, and J. Hescheler. 1999. Intracellular Ca^{2+} oscillations drive spontaneous contractions in cardiomyocytes during early development. *Proc. Natl. Acad. Sci. USA.* 96:8259–8264.

Vinogradova, T.M., Y.Y. Zhou, V. Maltsev, A. Lyashkov, M. Stern, and E.G. Lakatta. 2004. Rhythmic ryanodine receptor Ca^{2+} releases during diastolic depolarization of sinoatrial pacemaker cells do not require membrane depolarization. *Circ. Res.* 94:802–809.

Woo, S.H., L. Cleemann, and M. Morad. 2002. Ca^{2+} current-gated focal and local Ca^{2+} release in rat atrial myocytes: evidence from rapid 2-D confocal imaging. *J. Physiol.* 543:439–453.

Woo, S.H., L. Cleemann, and M. Morad. 2003. Spatiotemporal characteristics of junctional and nonjunctional focal Ca^{2+} release in rat atrial myocytes. *Circ. Res.* 92:e1–11.

Yang, H.T., D. Tweedie, S. Wang, A. Guia, T. Vinogradova, K. Bogdanov, P.D. Allen, M.D. Stern, E.G. Lakatta, and K.R. Boheler. 2002. The ryanodine receptor modulates the spontaneous beating rate of cardiomyocytes during development. *Proc. Natl. Acad. Sci. USA.* 99:9225–9230.